JOURNAL OF MATERIALS SCIENCE **37** (2002) 4431 – 4436

Nanostructured cation distribution in $FeNbO_4$: A synchrotron powder diffraction and transmission electron microscopy investigation

R. THEISSMANN, H. EHRENBERG, H. WEITZEL, H. FUESS
Darmstadt University of Technology, Institute for Materials Science, Petersenstr. 23, D-64287 Darmstadt, Germany
E-mail: theissmann@friedel.st.mw.tu-darmstadt.de

The real structure of $FeNbO_4$ was determined by a combination of electron microscopy investigations and high resolution synchrotron powder diffraction. It is shown that the order-disorder phase transition from the orthorhombic high-temperature modification (α-PbO_2-type structure) to the monoclinic low-temperature modification (wolframite-type structure) of $FeNbO_4$ is *translationengleich* and leads to a domain structure that consists of a coherent mixture of the orthorhombic and the monoclinic modification. Domains of the monoclinic phase are separated by antiphase boundaries with an antiphase vector $(\frac{1}{2},\frac{1}{2}\cdot 0)$. The real structures of eight different samples have been investigated in terms of domain size and degree of cation ordering by peak-shape analysis and the ratio between integrated intensities of split-structure and fundamental reflections. The obtained real structure is correlated with the conditions of synthesis.

1. Introduction

Possible applications for some types of ABO_4 oxides, e.g., $FeNbO_4$, $FeTaO_4$ and $FeWO_4$, as gas sensors [1–4], catalysts or in photodetector technology [5, 6] have given rise to an intensive study of these materials within the last decade. Special topics of interest are the electric and magnetic properties [4, 7–9] as well as new routes of synthesis [10–12]. Of primary importance for the understanding of the physical properties of these materials is a detailed knowledge of the underlying ideal and real structures. This paper presents the results of Rietveld refinements based on synchrotron powder diffraction data recorded for eight samples with the formal composition $FeNbO_4$ but prepared under different conditions. In the phase diagram Fe_2O_3-Nb_2O_5 four modifications with the formal composition $FeNbO_4$ are known [13–15]. In two of them Fe and Nb are randomly distributed on one crystallographic site, i.e., the notation $(Fe_{0.5}Nb_{0.5})O_2$ is more appropriate. At higher temperatures ($T > 1380$°C) the rutile-type structure with tetragonal symmetry (space group $P4_2/mnm$) is formed, while at lower temperatures the α-PbO_2-type structure with orthorhombic symmetry (space group *Pbcn*) is realized. In the latter ordering of the cations occurs between 1050 and 1100°C, resulting in a reduction of symmetry. This phase transition due to cation ordering is *translationengleich* [16] and leads to the wolframite-type structure (space group $P2/c$). The fourth modification is reported to be stable at 700°C and crystallizes in the $AlNbO_4$ type structure (space group $C2/m$) [14, 15]. In this paper it is shown that the ideal structure and the real structure of the samples can be controlled by the conditions of synthesis.

2. Sample preparation and experimental

The synthesis of $FeNbO_4$ powder samples was carried out by the sol-gel method [10]. $NbCl_5$ (Fluka, 99,9%) and $FeCl_3$*$6H_2O$ (Fluka, Assay 99–102%) were used as educts. The gel was dried at 250°C and characterized by X-ray powder diffraction on a Siemens D500 Bragg-Brentano diffractometer with Cu-K_α radiation and a secondary monochromator. Only gels without impurities have been used in the following process. The pure gel was divided into different samples, put in alumina crucibles and treated with different temperature programs. One sample *(Sample A)* was annealed at 1050°C for 12 hours and cooled down in air slowly to room temperature. One half of this sample was annealed again for 2 hours at 1150°C and quenched in water *(Sample I)*. All other samples were annealed at 1050°C for 12 hours, followed by 2 more hours at 1150°C and quenching in water. The as quenched samples were annealed again at temperatures of 700°C *(Sample B)*, 800°C *(Sample C)*, 950°C *(Sample D)*, 1000°C *(Sample E)*, 1040°C *(Sample F)*, 1060°C *(Sample G)* and 1080°C *(Sample H)* for 2 hours, see Table I. The synthesis of nonstoichiometric samples was tried by mixing and ballmilling of the dried gel together with small additional amounts of Fe_2O_3 or Nb_2O_5 between 1 and 10 wt%. These samples were annealed for 12 hours at 1050°C and 1150°C, respectively. All samples were characterized by X-ray powder diffraction. *Sample I* as well as *Sample A* and the nonstoichiometric samples

TABLE I The refined size parameter of Fullprof profile function no. 7, the calculated domain size and the measured TEM domain size of the *Samples A, C–I*

Temperature treatment	*Sample*	Ly	Domain size Scherrer (Å)	Domain size TEM	Degree of cation order (%)
1050°C, 12 h	*A*	0.0336(13)	2311(90)	Not measured	99(1)
1050°C 12 h, 1150°C 2 h, 700°C 2 h	*B*				
1050°C 12 h, 1150°C 2 h, 800°C 2 h	*C*	1.192(68)	35(3)	41(12) Å	55(3)
1050°C 12 h, 1150°C 2 h, 950°C 2 h	*D*	0.450(13)	98(5)	81(20) Å	77(4)
1050°C 12 h, 1150°C 2 h, 1000°C 2 h	*E*	0.210(3)	201(9)	Not measured	84(4)
1050°C 12 h, 1150°C 2 h, 1040°C 2 h	*F*	0.113(2)	373(15)	Not measured	80(2)
1050°C 12 h, 1150°C 2 h, 1060°C 2 h	*G*	0.092(2)	477(20)	437(63) Å	63(2)
1050°C 12 h, 1150°C 2 h, 1080°C 2 h	*H*	0.141(4)	300(18)	Not measured	39(2)
1050°C 12 h, 1150°C 2 h	*I*				0

were measured on a STOE STADI P diffractometer (Co-$K\alpha_1$) in transmission mode, all other samples were, in addition, measured at beamline B2 at the *Hamburger Synchrotronstrahlungslabor* HASYLAB, Germany. A pneumatically bent cylindrical mirror was used to optimize instrumental resolution by minimizing vertical divergence [17]. Wavelengths of 1.15962 and 1.20878 Å, respectively, were selected for the high-resolution diffraction experiments by a Ge(111) double-crystal monochromator. In addition, a Ge(111) analyzing crystal was used in front of the NaI scintillation counter. For the refinement of the crystal structure the software package Fullprof [18] was used. Transmission Electron Microscopy (TEM) investigations were carried out on a Philips CM20 and a Philips CM12 microscope. Contrast simulations were performed with the software package NCEMSS [19].

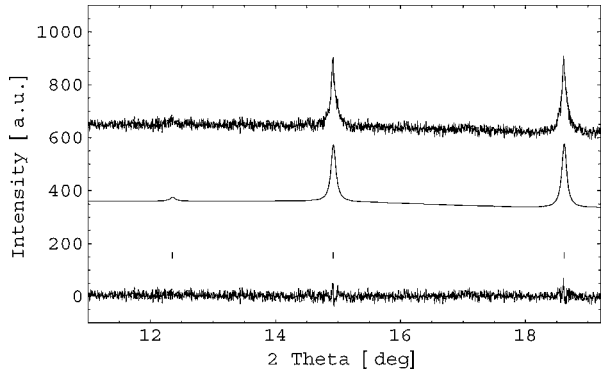

Figure 1 Section of an high-resolution synchrotron powder diffraction pattern of *Sample G* (top), calculated intensities based on crystal structure refinement (middle), and the difference between these patterns (bottom). The shown reflections are split-structure reflections with the indices (010), (100) and (011).

3. Analysis of data

The X-ray diffraction data for *Sample A* can be refined as a pure $FeNbO_4$ of wolframite-type structure. The atomic parameters are in good agreement with literature [13]. *Sample I* contains small amounts of hematite (about 0.8 weight%). The refinement of the structure of this sample reveals $(Fe_{0.5}Nb_{0.5})O_2$ with the α-PbO_2-type structure, the atomic parameters are again in good agreement with previous data [13]. In both samples no peak-shape anomalies were found. *Sample B* gave a diffraction pattern without any significant difference to the one of *Sample A* and was not further investigated. All other samples show significant peak shape anomalies. Strong broadening is obtained as well as asymmetries to higher and lower angles of diffraction. Crystallographic aspects have to be considered to explain these peak shape anomalies: The reduction of symmetry from the orthorhombic to the monoclinic polymorph of $FeNbO_4$, this order-disorder phase transition is *translationengleich*, is accompanied by a two-step symmetry reduction: 1. The distortion of the lattice with $\beta = 90^\circ \rightarrow \beta \neq 90^\circ$ without cation ordering, 2. cation ordering. The deviation of the monoclinic angle β from 90° results in a splitting of the crystallographic (8d)-site of the oxygen sublattice of the orthorhombic phase into two different (4g)-sites for the monoclinic polymorph. The crystallographic (4c)-site of the orthorhombic structure is randomly occupied by Fe and Nb and splits into the (2e)- and (2f)-sites of the monoclinic structure. Without cation ordering, both of these sites, (2e) and (2f), are occupied half by Nb and half by Fe. The symmetry reduction results in a splitting of the (h, k, l) reflections into $(h, k, +l)$ and $(h, k, -l)$ reflections. Due to the random distribution of the cations onto the (2e)- and (2f)-site, the loss of the reflection conditions $0kl : k = 2n$, $hk0 : h + k = 2n$, $(h00 : h = 2n)$, and $(0k0 : k = 2n)$, corresponding to the break of b and n glide plane symmetry, results in no additional detectable reflections, since their structure factors are close to zero. Reflections of this type are denoted split-structure reflections [20]; they gain intensity from cation ordering. The intensities and peak shapes of these reflections are directly related to the degree of cation order and further real structure pecularities of the samples. Peak shape analysis shows that broadening occurs for all split-structure reflections (Fig. 1), while asymmetries are found for fundamental reflections (Figs. 2 and 3). The patterns of all samples with such anomalies were fitted by contributions from both the orthorhombic and the monoclinic modification. Furthermore, a splitting of the pattern of the monoclinic modification into two different contributions was necessary, according to the crystallographic aspects discussed: The split-structure reflections were described by a different peak shape as compared with the fundamental reflections. All refinements were based on fixed background points with a linear interpolation in between. The refined parameters are the metric of the unit cells, atomic positions, isotropic temperature

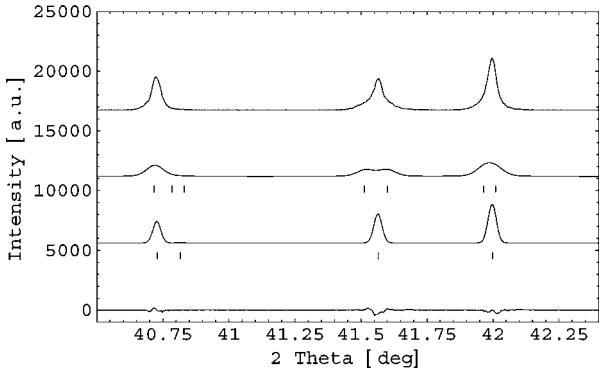

Figure 2 Section of an high-resolution synchrotron powder diffraction pattern of *Sample G* (top), calculated contribution of the wolframite-type phase to the fundamental reflections based on crystal structure refinement (2nd), calculated contribution of the α-PbO_2-type phase based on crystal structure refinement (3rd), and the difference between the total calculated and observed profiles (bottom).

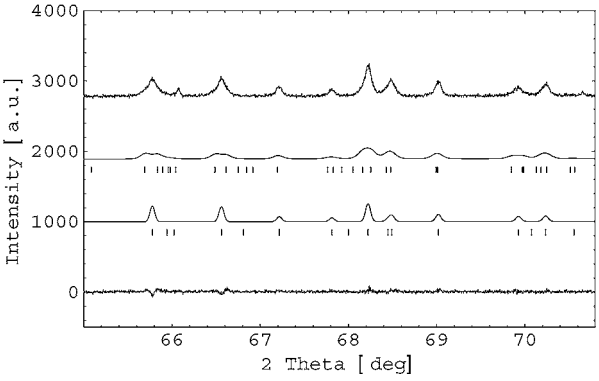

Figure 3 Section of an high-resolution synchrotron powder diffraction pattern of *Sample G* (top), calculated contribution of the wolframite-type phase to the fundamental reflections based on crystal structure refinement (2nd), calculated contribution of the α-PbO_2 type phase based on crystal structure refinement (3rd), and the difference between the total calculated and observed profiles (bottom).

factors, the iron-niobium distribution onto the (2e)- and (2f)-sites, and the peak shape (profile function no. 7). The lattice constants for all phases are in good agreement with published data, see Tables II and III. Table IV gives the atomic parameters, again in good agreement with published data [13]. Peak-shape analysis of the split-structure reflections implies a dependence of the FWHM on a size effect, since they can be fitted very well with the Scherrer parameter Ly in Fullprof [18]. The domain sizes of the samples are listed in Table I. Furthermore, the peak-shape analysis shows that *Samples C, D, E* show a Lorentzian shape for the fundamental reflections of the wolframite-type phase while the corresponding peaks of *Samples F, G, H* are mainly of Gaussian shape. For all samples heated above the temperature of the orthorhombic-monoclinic phase transition, small amounts of hematite with a maximum content of 0.8 wt% could be found within the samples. This occurence of impurities is in agreement with published observations [5, 8, 23]. However, in contrast to all the other studies on $FeNbO_4$ cited before, no indication for $FeNb_2O_6$ with columbite-type structure was found in any of the samples under investigation. All attempts to obtain non-stoichiometric samples resulted in an increased amount of the correspoding oxide Fe_2O_3 or Nb_2O_5 as impurity.

TABLE II Lattice parameters of the wolframite-type phase in comparions with data from literature

Sample	a/Å	b/Å	c/Å	β/°
A	4.65028(11)	5.61564(11)	4.99778(11)	90.149(2)
C	4.65231(6)	5.61521(6)	5.00281(6)	89.991(4)
D	4.65108(10)	5.61535(10)	4.99752(7)	90.010(3)
E	4.65242(19)	5.61887(23)	4.99983(19)	90.134(6)
F	4.65284(8)	5.61773(10)	5.00117(8)	90.124(3)
G	4.65320(7)	5.61720(6)	5.00214(7)	90.109(2)
H	4.65331(12)	5.61555(14)	5.00276(12)	90.098(4)
[21]	4.653	5.620	5.001	90.16
[8]	4.6560(3)	5.6319(3)	5.0076(2)	90.27(7)
[4]	4.649	5.623	5.006	90.4

TABLE III Lattice parameters of the α-PbO_2-type phase in comparison with data from literature

Sample	a/Å	b/Å	c/Å
C	4.65010(4)	5.61787(6)	4.99907(6)
D	4.64926(5)	5.61737(5)	4.99765(5)
E	4.65116(6)	5.61679(6)	4.99857(6)
F	4.65201(5)	5.61670(5)	5.00071(5)
G	4.65244(6)	5.61627(6)	5.00164(6)
H	4.65206(2)	5.61698(2)	5.00333(2)
I	4.65523(10)	5.61877(10)	5.00875(10)
[21]	4.647	5.613	5.005
[22]	4.6496(1)	5.6181(1)	5.0058(1)
[12]	4.651(5)	5.613(5)	5.004(5)
[8]	4.6616(2)	5.6329(2)	5.0164(2)

TABLE IV Fractional coordinates of the (4c)- and (8d)-sites of the orthorhombic modification and of the (2e)-, (2f)- and (4g)-sites of the monoclinic modification

Crystallographic site	Atoms	x	y	z
4c	Fe/Nb	0	0.1768(6)	$\frac{1}{4}$
8d	O	0.267(7)	0.3861(2)	0.417(5)
2e	Fe	0	0.1713(24)	$\frac{1}{4}$
2f	Nb	$\frac{1}{2}$	0.6799(7)	$\frac{1}{4}$
4g	O	0.225(16)	0.118(7)	0.911(3)
4g	O	0.298(12)	0.382(7)	0.437(11)

The given values are averages for all samples with standard deviations in brackets.

TEM dark-field imaging was applied to split-structure reflections and, for comparison, also to fundamental reflections on several samples. A domain structure can clearly be seen in the dark-field images as the light areas represent cation order and dark areas cation disorder (Fig. 4). High-resolution TEM images of areas that contain boundaries from one monoclinic to another monoclinic area show that a perfectly ordered oxygen sublattice is preserved (Fig. 5). The lattice constant of the orthorhombic phase along b appears with only half the value as compared to the lattice constant of the monoclinic domains due to the additional *b*-glide planes. Lattice planes in neighboured monoclinic domains are shifted by half of the lattice constant along b corresponding to the anti-phase vector $(\frac{1}{2},\frac{1}{2}, 0)$ for this projection. High-resolution contrast simulations were calculated for both the monoclinic and the orthorhombic modification. Therein the difference between the orthorhombic and the monoclinic phase can be seen by a virtual bisecting of the lattice constant for the

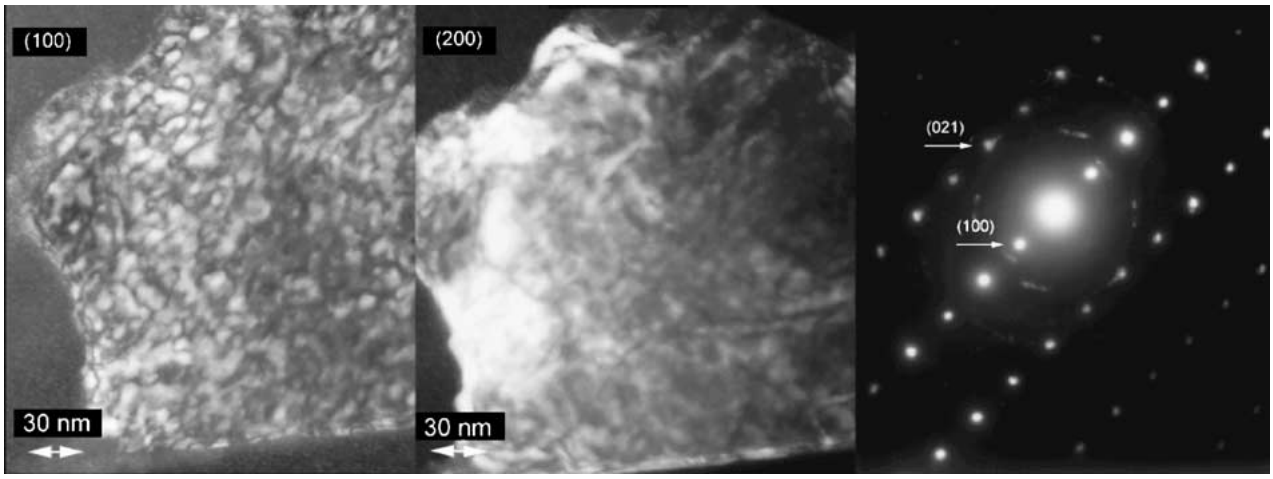

Figure 4 TEM dark-field and small-area electron diffraction (SAED) images of *Sample D*. (200) is a fundamental reflection, while (100) is a split-structure reflection.

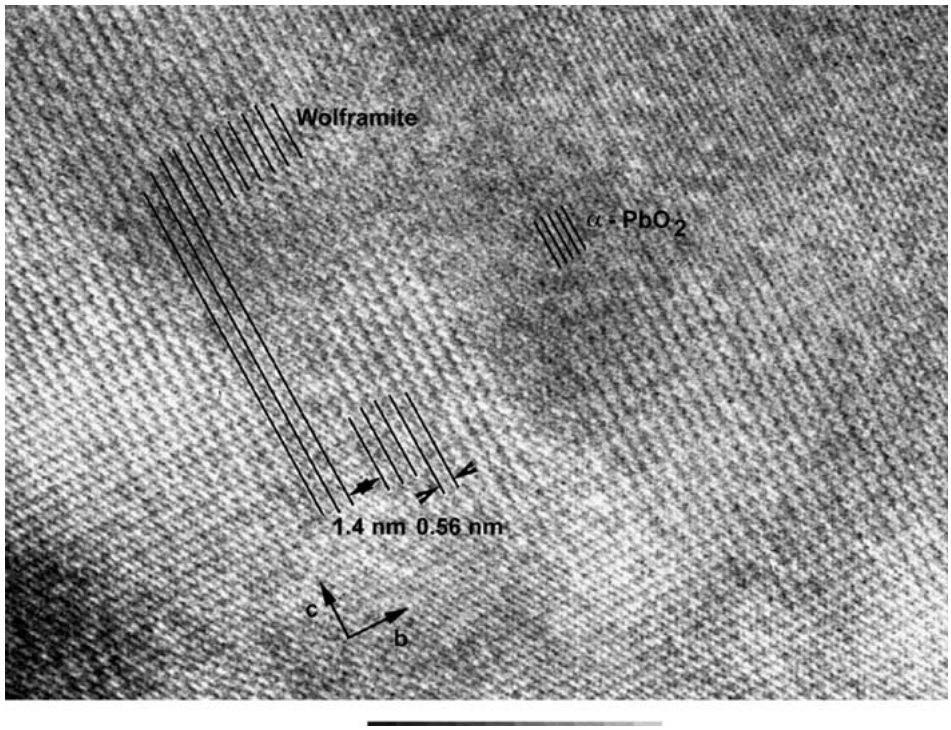

Figure 5 High-resolution TEM image of *Sample F*. The orthorhombic modification can be distinguished from the monoclinic modification by a virtual bisecting of the lattice constant of the monoclinic phase in the orthorhombic phase. The antiphase correlation between two separated monoclinic areas can be seen by the shift about half a lattice constant along b, caused by 2.5 unit cells of the othorhombic modification (1.40 nm).

orthorhombic phase as compared to the monoclinic modification. This reflects the different projection properties of a 2-fold axis compared to a *b*-glide plane. The simulation was calculated for a series of defocus values from −400 Å to 200 Å in steps of 50 Å and for different sample thicknesses from 100 Å to 300 Å in increments of 40 Å. The change from one monoclinic domain to the next matches the result of the simulation as the monoclinic domains are separated by several atomic layers of the orthorhombic modification and a specific shift in the lattice.

Refinements based on the synchrotron and laboratory X-ray powder diffraction data were performed to quantify the degree of cation disorder for different samples. The applied Rietveld method optimizes model parameters with respect to all individual data points and not only integrated intensities, so that peak overlap and profile analysis are most properly taken into account. A promising model has to be based on the nanostructured cation distribution and must reproduce the observed peak shapes. Three kinds of contributions to the observed profiles have been distinguished: (1) The split-structure reflections are due to the undisturbed cation order in domains with wolframite-type structure and appear as very broad reflections because of the small domain size. (2) Fundamental reflections of the wolframite phase are much sharper as they result from much larger domains. Antiphase boundaries within these domains affect only the intensities but not the half-width of fundamental reflections as they do not destroy coherence. (3) Areas with a random distribution of cations contribute only to fundamental reflections, but according to the orthorhombic α-PbO_2-type structure there is no splitting between reflections (h, k, l)

and $(h, k, -l)$. Formally, these three contributions are treated as separate phases with constrained structural parameters. The isotropic thermal displacement parameters of all oxygens in all phases were constrained to the same value. Furthermore, the structural parameters for the wolframite-type phase were constrained, although the corresponding reflections were formally split into the two sets of split-structure reflections on one hand and fundamental reflections on the other with different peak shapes and half widths. The degree of cation order, as listed in Table I, is deduced from the ratio of the integrated intensities of the split-structure reflections compared to those of the fundamental reflections. 100% cation order corresponds to the ideal wolframite-type structure, 0% represents complete cation disorder, i.e., the α-PbO_2-type structure. The reliability of this refinement procedure is severely cross-checked by the agreement of bond lengths and angles with typcial values for $[FeO_6]$- and $[NbO_6]$-octahedra. All isotropic thermal displacement parameters converged to positive and meaningful values.

4. Results

All synthesized $FeNbO_4$ samples show a significant broadening of the split-structure reflections due to the domain structures of the samples. The domains are distinguished from each other by the occupation of the crystallographic (2e)- and (2f)-sites with iron and niobium, respectively. This interchange within an undisturbed oxygen sublattice causes antiphase correlations between two monoclinic domains with an antiphase vector $(\frac{1}{2},\frac{1}{2}, 0)$. *Samples C* and *D* do not show complete cation ordering within the wolframite-type phase. It is concluded that the process of cation ordering occurs from several crystallization germs within the sample. The chosen annealing conditions for all wolframite samples did not lead to a sample of pure wolframite phase. The growth of the crystallization germs is therefore very slow and disturbed by the surrounding germs, that themselves have the same tendency of growing. The ordering process goes along with a distortion of the oxygen sublattice, which is denoted to be the reason of the Lorentzian peak shape of the samples mentioned above. *Samples F, G and H* were quenched from temperatures at or near the phase transition and do not show a distortion of the oxygen sublattice, but a peak shape, related to domain size effects. The synthesis of $FeNbO_4$ with a perfect wolframite-type structure can probably be realised from a highly sintering active $FeNbO_4$ gel with tempering times of several days at temperatures below 1050°C. The presence of hematite in all samples, that were annealed at temperatures above the monoclinic → orthorhombic transition temperature, and its increasing amount with longer periods of tempering, suggests that the orthorhombic modification of $FeNbO_4$ is only metastable against decomposition. Quenching of samples from temperatures above the stability range of the monoclinic modification freezes the metastable orthorhombic modification at room temperature. Therefore, the stability range for non-stoichiometric samples prepared by this method must be very narrow (less than 1%).

5. Discussion

The existence of a nanostructured cation distribution in $FeNbO_4$ was investigated on three different length scales. The high-resolution TEM images show that the nanostructure is caused by antiphase boundaries with an antiphase vector $(\frac{1}{2},\frac{1}{2},0)$ on bond length scale. Dark-field imaging of $FeNbO_4$ crystallites shows the homogeneous distribution of the antiphase boundaries on a scale of microns over single grains of the sample. X-ray diffraction gives an average information, which is representative for the whole sample. Even if the model for the real structure used for the Rietveld refinement is too simple as the regions with α-PbO_2-type and wolframite-type structures are treated separately and possible phase correlations are neglected, it provides a very successful description of the microstructure of the sample. The influence of annealing temperature on domain size and cation order is reliable, however, the absolute numbers for the degree of cation order are not unambigously defined. The good agreement of domain size calculations based on $a1/\cos\Theta$ dependent Lorentzian broadening and on TEM results support the derivation of domain sizes from the broadening of the split-structure reflections.

The existence of different kinds of real structures is a consequence of different sample preparation conditions. *In situ* experiments at high temperature could show whether the monoclinic → orthorhombic order-disorder phase transition is of second order at thermal equilibrium or not. In any case the samples possess a well pronounced real structure at room temperature. But it cannot be excluded that at high temperature the disorder is restricted on diffusion of Fe- and Nb-ions one with another without the formation of particular Fe- and Nb-layers, going along with unbroadened split-structure reflections at these temperatures. Only in that case the order-disorder phase transition would be of second order.

Based on these results, an interpretation of the physical properties of $FeNbO_4$ and its possible applications becomes promising and is in progress now with respect to the electric and magnetic properties.

Acknowledgement

Financial support by the *Deutsche Forschungsgemeinschaft* under grant-no. WE 1542/4-1,2 and the *Fonds der Chemischen Industrie* is gratefully acknowledged. The performance of transmission electron microscopy and the interpretation of results have been supported considerably by Dr. G. Miehe.

References

1. D. H. DAWSON and D. E. WILLIAMS, *J. Mater. Chem.* **6** (1996) 409.
2. G. S. HENSHAW, L. MORRIS, L. J. GELLMAN and D. E. WILLIAMS, *ibid.* **6** (1996) 1883.
3. C. CANTALINI, H. T. SUN, M. FACCIO, G. FERRE and M. PELINO, *Sensors and Actuators* B **24/25** (1995) 673.
4. K. I. GNANASEKAR, V. JAYARAMAN, E. PRABHU, T. GNANASEKARAN and G. PERIASWAMI, *ibid.* **55** (1999) 170.
5. H. LEIVA, K. SIEBER, B. KHAZAI, K. DWIGHT and A. WOLD, *J. Solid State Chem.* **44** (1982) 113.

6. Y. NODA, M. SHIMADA, M. KOIZUMI and F. KANAMARU, *ibid.* **28** (1979) 379.
7. H. EHRENBERG, G. WLTSCHEK, R. THEISSMANN, H. WEITZEL, H. FUESS and F. TROUW, *J. Magn. Magn. Mater.* **218** (2000) 261.
8. E. SCHMIDBAUER and J. SCHNEIDER, *J. Solid State Chem.* **134** (1997) 253.
9. E. SCHMIDBAUER, *J. Phys.: Condens. Matter* **10** (1998) 8279.
10. M. A. TENA, E. CORDONCILLO, G. MONROS, J. CARDA and P. ESCRIBANO, *Mater. Res. Bull.* **30** (1995) 933.
11. M. A. TENA, G. MONROS, J. CARDA, V. CANTAVELLA and P. ESCRIBANO, *J. Sol-Gel Science and Techn.* **2** (1994) 381.
12. G. POURROY, A. MALATS, I. RIERA, P. POIX and R. POINSOT, *J. Solid State Chem.* **88** (1990) 476.
13. H. WEITZEL and H. SCHRÖCKE, *N. Jahrb. Miner. Abhandl.* **119** (1973) 285.
14. H. BRUNNER and R. GRUEHN, *Z. Naturforsch.* **31b** (1976) 318.
15. M. HARDER and HK. MUELLER-BUSCHBAUM, *Z. Anorg. Allg. Chem.* **456** (1979) 99.
16. International Tables for Crystallography, vol. A. edited by T. Hahn (Kluwer Academic Publishers, 1995) p. 727.
17. M. KNAPP, H. EHRENBERG, H. FUESS, U. HAHN, M. HESSE, H. SCHULTE-SCHREPPING and T. WROBLEWSKI, *Nucl. Instr. Meth.* A **467/468** (2001) 291.
18. J. RODRIGUEZ-CARVAJAL, Abstracts of the Satellite Meeting of the XV. Congress of the International Union of Crystallography, Toulouse, 1990 p. 127.
19. R. KILAAS, in Proc. 45th Annual Meeting EMSA (1987) p. 66.
20. F. LAVES, G. BAYER and A. PANAGOS, *Schweiz. Mineral. Petrograph. Mitt.* **43** (1963) 217.
21. R. S. ROTH and J. L. WARING, *Amer. Miner.* **49** (1964) 140.
22. W. T. A. HARRISON and A. K. CHEETHAM, *Mater. Res. Bull.* **24** (1989) 523.
23. J. KOENITZER, B. KHAZAI, J. HORMADALY, R. KERSHAW, K. DWIGHT and A. WOLD, *J. Solid State Chem.* **35** (1980) 128.

Received 17 October 2001
and accepted 15 May 2002